Carbon molecular sieve hollow fiber membranes derived from dip-coated precursor hollow fibers comprising nanoparticles

Yuhe Cao [1], Kuang Zhang [1], Chen Zhang [2], William J. Koros [1]*

1 School of Chemical and Biomolecular Engineering, Georgia Institute of Technology, Atlanta, GA, 30332, USA

2 Department of Chemical and Biomolecular Engineering, University of Maryland, 4418 Stadium Dr. College Park, MD 20742, United States

*Correspondence

William J. Koros, School of Chemical & Biomolecular Engineering, Georgia Institute of Technology, 311 Ferst Drive, Atlanta, GA 30332.

Email: wjk@chbe.gatech.edu

Present address

Yuhe Cao, Ralph E Martin Department of Chemical Engineering, University of Arkansas, Fayetteville, AR 72701, United States

Abstract

We report a novel approach to economically fabricate dual-layer composite nanoparticle-containing carbon molecular sieve (CMS) hollow fiber membranes having excellent gas separation performance. The economically favored process comprises dip coating engineered support layer fibers to form a dense skin layer in a CMS precursor. The coated fibers are then pyrolyzed to form a high-performance CMS hollow fiber membrane. The nano-particle containing composite carbon molecular sieve hollow fiber membranes showed very attractive selectivities and productivities. This work shows how to produce high performance CMS hollow fiber membrane by coating, which exceeds that achieved with the standard sol-gel support stabilization technique.

Keywords: Carbon molecular sieve; Hollow fiber membranes; Dip coating; Nanoparticle; Natural gas purification

1. Introduction

Carbon molecular sieve (CMS) membranes in a dense film configuration have shown separation performance surpassing the polymeric upper bound for a variety of gas pairs such as O_2/N_2 [1], CO_2/CH_4 [2], CO_2/CH_4 [3], C_2H_4/C_2H_6 [4], C_3H_6/C_3H_8 [5] etc. However, CMS hollow fiber membranes are preferred for large scale applications due to their ability to be formed into compact modules with high surface area-to-module volume ratios. Unfortunately, since the pyrolysis occurs above the polymer glass transition temperature (Tg), partial or even total collapse of the porous core layer can occur. This collapse creates a thick separation layer with low permeance, and is therefore, much less productive than would be expected if the collapse could be avoided.

Several approaches were attempted to mitigate the substructure collapse problem. Chemical crosslinking was attempted to restrict the bulk polymer flow throughout pyrolysis. One approach that had been applied to crosslink polyimides was the use of diamine linkers, where the diamine reacts with imides to open the ring and form an amide bond. Diamine crosslinking did not work for restricting collapse due to the instability of the amide (-CONH) bond at higher temperatures [6]. Xu et al. [7] observed that the 6FDA based polymer precursors exhibited a lower degree of substructure collapse compared to Matrimid® precursor because of the rigid structure and higher Tg. CMS hollow fibers from 6FDA:BPDA-DAM exhibited a lower degree of collapse, but still a significant amount of densification in membrane skin thickness was observed. This densification leads to CMS with poor permeances and significantly thicker separation layer (at least one order of magnitude) [8]. Bhuwania and co-workers [9] made a breakthrough in fabricating thin-skinned CMS hollow fiber membranes by using in situ sol-gel reaction. vinyltrimethoxysilane (VTMS) was introduced to the precursor fiber by soaking, followed by a moisture-induced hydrolysis and condensation. A cross-linked silica network was formed, and it can effectively suppress the support densification. However, the VTMS on the fiber skin layer can add nonselective mass transfer resistance to permeation.

Alternative stabilization can be achieved by making nanoparticle-filler-containing support layer fibers [8]. The nanoparticle-filler containing support layers showed attractive features. The silica

particles with low bulk density were dispersed in the support layer of polymer precursor hollow fibers and spun in a sheath-core format using the same (Matrimid®) sheath and nanoparticle core precursor polymer. The resultant composite CMS membrane showed higher performance than those of monolithic asymmetric CMS membranes formed by the standard sol-gel support stabilization technique [8]. However, defect-free precursor fiber membranes need to be spun prior to the CMS formation. Other approaches to form composite CMS membranes rely upon robust but expensive ceramic or metal porous support layer [10, 11]. During the fabrication process, a thin skin layer of polymer can be formed by coating prior to pyrolysis to obtain both high selectivity and permeance of resultant CMS fibers. However, fabricating such support membranes is relatively more complicated and costly than spinning hollow fiber.

In this work, we demonstrate the dip-coating approach to fabricate the nanoparticle-containing composite CMS membrane with a different sheath and nanoparticle containing core. There is no need to spin defect-free precursor fiber—which greatly decreases the spinning difficulty. Compared with the monolithic CMS, the CMS via coating showed excellent CO_2/CH_4 performance in terms of selectivity and permeance. For instance, a 10 % v-treated monolithic 6FDA: BPDA-DAM at 675 °C gives 100 GPU CO_2 permeance with CO_2/CH_4 selectivity of 70, which is less than the CMS-800 in this article, which also has higher selectivity).

The approach in the current workshows a costly high performance polymer (e.g. 6FDA: BPDA-DAM, 6FDA-DAM: DABA (3:2) polymer) and a low cost support precursor polymer (e.g. P84®) can be used to fabricate the support and minimize cost of the composite membrane. Carefully selected commercially available silica particles were dispersed in the precursor hollow fiber's porous support layer and shown suitable to maintain high permeance without using VTMS treatment of precursor fibers [12].

2. Materials and methods

2.1 Materials

The coating copolyimide polymer 6FDA:BPDA-DAM (1:1) was synthesized via condensation reaction between 4,4'-(Hexafluoroisopropylidene) diphthalic anhydride (6FDA) and 3,3'-4,4'-biphenyl tetracarboxylic dianhydride (BPDA) with 2,4,6-trimethyl-1,3-phenylene diamine (DAM). First we form a high molecular weight polyamic acid at low temperatures and then perform a chemical imidization step, the specifics of which are described elsewhere [13]. A commercial thermoset copolyimide, P84® (BTDA-TDI/MDI, copolyimide of 3,3′4,4′-benzophenone tetracarboxylic dianhydride and 80% methylphenylene-diamine + 20% methylene diamine; HP Polymer GmbH, Austria) was chosen as a precursor in this work. The 6FDA-DAM: DABA (3:2) polymer (repeating unit shown in Fig. 1) used in this study was purchased from Akron Polymer Systems. The structures of the precursor material are shown in Fig. 1 [14]. Commercial silicon dioxide nanoparticles (Product # US3448, US Research Nanomatertials, Inc.) were utilized to make the support layer hollow fiber. The silane-treated silicon dioxide nanoparticles have a bulk density of 0.056 g/cm^3 with 15 nm average particle size. The particles were fluffy, and a large portion of the total amount of NMP solvent used was needed to disperse the dried nanoparticles initially. Then a NMP solution containing about 10 wt.% of the total

polymer was firstly added into the silicon dioxide dispersion. The remaining solvent and the dried polymer solids were then added to make dopes of the desired composition. The nanoparticle dispersion step was critical and the amount of the nanoparticle was limited by the NMP solvent availability. We need to make sure there was no visible agglomerates. The 6.7 wt.% was decided by observations during the dope preparation. We assume the higher concentration might need more effects to prepare a dope with nanoparticle dispersed evenly and could be considered in future studies.

Sure-seal bottles of hexane, 1-methyl-2-pyrrolidine (NMP), ethanol, tetrahydrofuran (THF) and acetone were purchased from Sigma-Aldrich (St Louis, MO). Methanol (20 L) and hexane (20 L) were purchased from BDH Chemicals Co. Pure-component CO_2 and CH_4 gases (Research Grade Quality) were purchased from Airgas (Radnor Township, PA), while 50:50 CO_2:CH_4 mixed gas (± 1% blend accuracy) was purchased from Nexair (Memphis, TN). All fittings used for module making were purchased from Swagelok® Georgia.

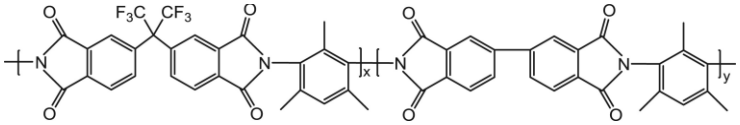

6FDA: BPDA-DAM (X=1; Y=1)
6FDA: 4,4'-(Hexafluoroisopropylidene) diphthalic anhydride
BPDA: 3,3'-4,4'-biphenyl tetracarboxylic dianhydride
DAM: 2,4,6-trimethyl-1,3-phenylene diamine

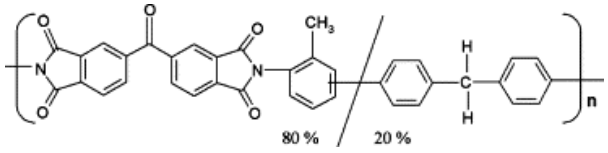

BTDA-TDI/MDI
BTDA: 3,3′4,4′-benzophenone tetracarboxylic dianhydride
TDI: toluene diisocyanate (methylphenylene-diamine)
MDI: methylene diamine

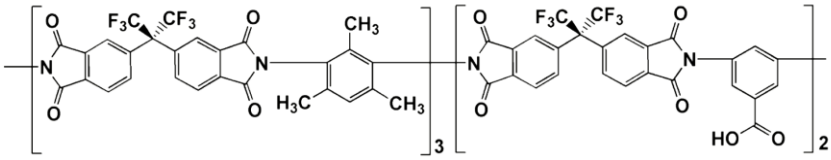

6FDA-DAM:DABA(3:2)
6FDA: 4,4'-(Hexafluoroisopropylidene) diphthalic anhydride
DAM: 2,4,6-trimethyl-1,3-phenylene diamine
DABA: 3,5-diaminobenzoic acid

Fig. 1. Chemical structure of the repeat units of 6FDA: BPDA-DAM, P84® (BTDA-TDI/MDI), and 6FDA-DAM:DABA(3:2) [14, 15].

2.2. Spinning of precursor hollow fiber supports comprising silica nanoparticles

Silicon dioxide nanoparticles were first dried in a vacuum oven at 180 °C overnight to remove moisture prior to being dispersed in NMP. A sonication bath was used to assist the nanoparticle dispersion, and sonication was stopped when no visible agglomerates could be observed. NMP

solution containing 10 wt% of the total P84® polymer was slowly added to the silicon dioxide dispersion. The remaining solvent and dried polymer solids were then added to provide the core spinning dope. The core spinning dope was co-extruded with a sheath spinning solution (P84® dissolved in NMP) and a bore fluid by a composite spinneret in a dry-jet/wet-quench spinning apparatus (Fig. 2A) to provide dual-layer composite hollow fibers [14]. The dual-layer composite hollow fibers comprise a P84® sheath layer on top of a porous P84® core layer comprising SiO_2 nanoparticles. Table 1 and 2 show the spinning dope compositions and spinning parameters, respectively.

Table 1. Dope composition of core spinning dope and sheath spinning dope to spin P84®/(SiO_2 + P84®) dual-layer fiber membranes.

Dope composition of core spinning dope and sheath spinning dope to spin P84®/(SiO_2 + P84®) dual-layer fiber membranes.		
	Dope composition	
	Core (SiO_2 + P84®)	sheath(P84®)
Component	wt.%	wt.%
polymer	25.9	32.2
NMP	67.4	50.5
SiO_2	6.7	0
THF	0	17.3

Table 2. Spinning parameters for hollow fiber membranes.

Spinning conditions for P84®/(SiO_2 + P84®) dual-layer fiber membranes.	
Spinning parameter	Value
Sheath dope flow rate	30 mL/h
Core dope flow rate	600 mL/h
Bore fluid flow rate	200 mL/h
Bore fluid composition	90 wt.%/10 wt.% NMP/H_2O
Take-up rate	5 m/min
Quench bath temperature	50 °C
Spinneret temperature	65 °C
Air gap height	18 cm

After spinning, the fibers were soaked in water baths for 3 days to remove the residual solvents. The fibers were then solvent exchanged in glass containers with three separate 20 min methanol baths followed by three separate 20 min hexane baths and dried under vacuum at 75 °C for 3 h. Prior to coating, the CO_2 permeance was 1079.6 GPU and the CO_2/CH_4 selectivity was 0.7. when tested with 50:50 CO_2:CH_4 mixed gas at 35 °C using 100 psi.

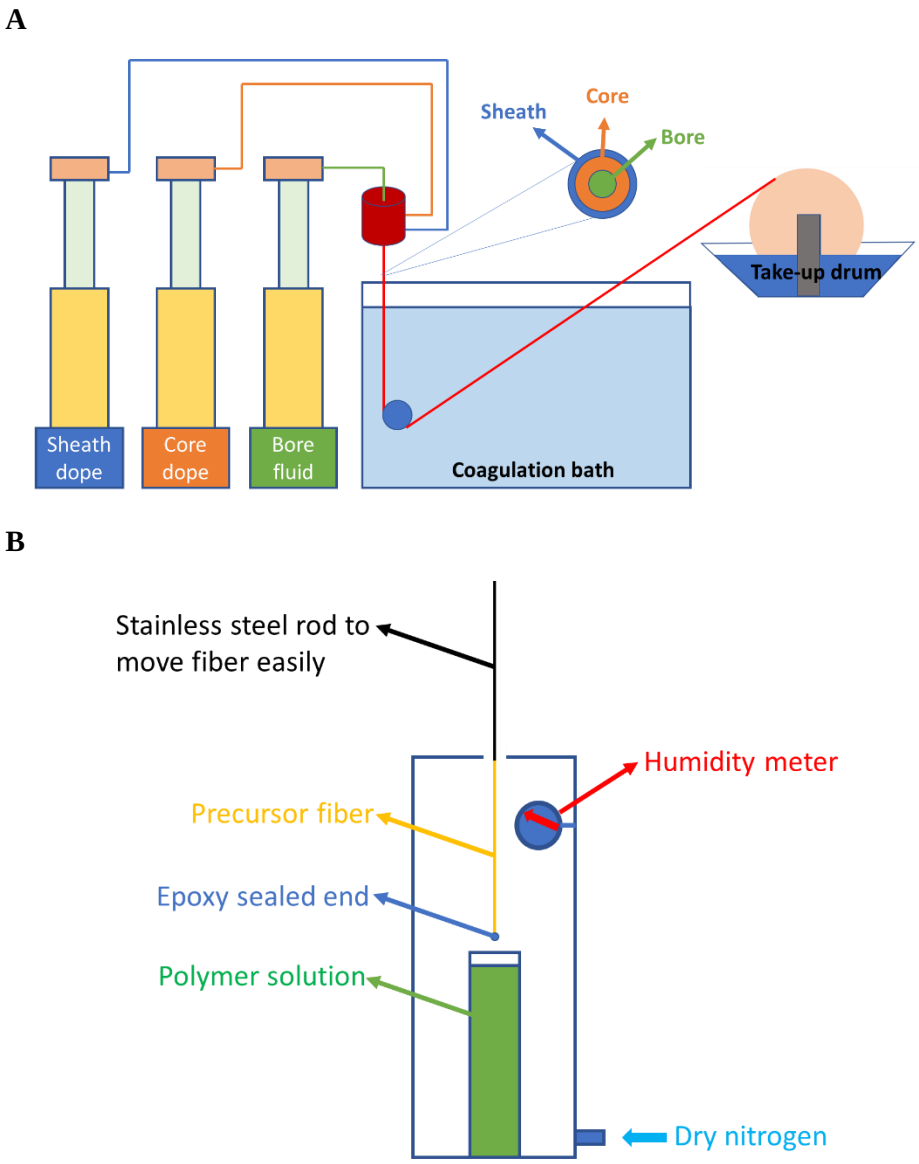

Fig. 2. (A) Dry-jet/wet-quench process for producing precursor hollow fiber membranes; (B) dip-coating of hollow fiber membrane in the chamber [14].

2.3 Coating of the precursor hollow fiber membrane

Polymer solutions were prepared comprising of 2-5 wt. % polymer (6FDA:BPDA-DAM or 6FDA-DAM:DABA (3:2)) dissolved in tetrahydrofuran (THF, Sigma-Aldrich Inc., 99.5%). A homogeneous coating solution without bubbles was formed after one day. A dip-coating method was applied to coat the polymer solutions onto the outer surface of the hollow fibers, which followed the protocol we developed previously [14]. As is shown in Fig. 2B, one end of the fiber was sealed by epoxy to prevent the solution from entering the lumen side. Coating of polymer on the precursor hollow fiber membrane was carried out by dipping the precursor in the polymer

solution for 30s. The fiber was taped onto a stainless steel rod to move the fiber in and out of the coating solution and evaporation zone. The dip-coated hollow fibers were dried under vacuum at 75 ° C for 2 hours. The dip-coating was carried out at high relative humidity (RH) of 60% (in atmosphere) or low RH of 10% (in a coating chamber purged by dry nitrogen, Fig. 2B).

2.4 Formation of CMS hollow fiber membranes by pyrolysis

CMS hollow fiber membranes were formed in a three-zone furnace (Thermcraft, Inc., model XST-3-0-24-3C) connected to a multichannel temperature controller (Model # CN1507TC, Omega Engineering Inc. Stanford, CT), which can achieve a uniform pyrolysis zone [7, 14]. The fibers were placed on a stainless-steel wire mesh (McMaster Carr, Robbinsville, NJ) and loaded into a quartz Tube (National Scientific Co. Quakertown, PA). Both ends of the quartz tube were sealed by an assembly of a metal flange with Silicon O-rings (Model # EQ-FI-60, MTI Corporation, Richmond, CA). The entire system was purged with ultrahigh purity (UHP) argon for at least 12 h to achieve reduce O_2 level in the system to below 1 ppm. Pyrolysis was performed using the heating protocol below under continuous purge of UHP argon (200 cc/min) [14],

1) 50 → 250 °C at a ramp rate of 13.3 °C/min
2) 250 °C → (T_{max}−15) °C at a ramp rate of 3.85 °C/min
3) (T_{max}−15) °C → T_{max} °C at a ramp rate of 0.25 °C/min
4) Soak for 2 h at T_{max} °C
5) Cool naturally to room temperature under UHP argon

where, T_{max}, is final pyrolysis temperature (550 °C, 675°C, and 800 °C). To achieve higher performance, a "thermal soak" process was added into the pyrolysis protocol for the 6FDA-DAM:DABA (3:2) coated precursor membranes as follows [16, 17],

1) 50 – 250 °C at a ramp rate of 13.33 °C/min
2) 250 – 370 °C at a ramp rate of 3.85 °C/min
3) 60 min thermal soak for cross-linking reaction at 370 °C
4) 370 – 675 °C at a ramp rate of 3.85 °C/min
5) 120 min thermal soak at 675 °C
6) Cool naturally to room temperature under UHP argon

After the pyrolysis, the resultant CMS fibers were removed from the furnace and used for subsequent characterization. Membrane modules were constructed using Scotch-Weld DP-100 epoxy resin (3 M Corporation) using procedures described elsewhere [18].

2.5 Gas Permeation Measurements

Mixed gas permeation tests were performed using a constant-pressure system in a temperature-controlled enclosure at 35 °C [14]. A 50 mol% CO_2 and 50 mol% CH_4 binary mixture with a constant pressure of 200 psi was introduced to the shell-side of the hollow fiber membranes with the bore-side presser of 1 atm. The permeate flow was measured by a bubble meter, and

composition was analyzed by a gas chromatograph (Varian 450-GC) after achieving the steady state to calculate the selectivity. The retentate flow rate was 100 times higher than the permeate flow rate to achieve 1% stage cut and to eliminate any effects of concentration polarization. Replicates were tested for all conditions described in the subsequent sections to ensure data reproducibility. The permeance (P/L) can be calculated using the following equation 1:

$$\frac{P}{L} = 10^{-6} \cdot \frac{Q_P \cdot 273.15}{A \cdot T \cdot \Delta p \cdot 5.17} \quad (1)$$

where P is permeability (give unit), L is membrane thickness (give unit), Q_p is the permeate flow rate in mL/sec, A is the active membrane area in cm^2, T is the room temperature in Kelvin, Δp is the transmembrane pressure difference in psia. The calculated permeance is in "Gas Permeation Units" (GPU) defined as:

$$1\ \text{GPU} = 1 \times 10^{-6}\ \frac{cm^3(stp)}{cm^2 \cdot s \cdot cmHg} \quad (2)$$

To characterize the separation performance of a hollow fiber membrane, two key factors, termed as permeance and selectivity, can be considered. The permeance, P_i/L, represents the separation productivity of a hollow fiber membrane and is defined as the flux of penetrant i normalized by the partial pressure or fugacity difference across the membrane, as shown in Equation 3,

$$\frac{P_i}{L} = \frac{n_i}{\Delta p_i} \quad (3)$$

In equation 3, P_i represents the permeability of penetrant i; L describes the effective membrane thickness; n_i represents the flux of penetrant i through the membrane; Δp_i refers to the partial pressure or fugacity difference of each penetrant across the membrane. The selectivity, α_{ij}, measures the membrane separation efficacy for a gas pair under conditions where the upstream pressure is much greater than the downstream. It is defined by the ratio of the fast gas (i) permeance to the slow gas (j) permeance, as shown in Equation 4,

$$\alpha_{ij} = \frac{P_i/L}{P_j/L} \quad (4)$$

2.6. Membrane morphology characterizations

Zeiss Ultra60 Fe-SEM was used to characterize the morphologies of polymer precursor hollow fibers and CMS hollow fibers. Polymer precursor samples were prepared by immersion in hexane followed by fracturing in Liquid Nitrogen. CMS samples were prepared by simply fracturing them by hands. All samples were put on a carbon tape and attached on suitable SEM stubs. The polymer samples were sputter coated with gold using Hummer 6 Gold/Palladium Sputterer for 5 min to avoid sample charging. CMS samples did not require any sputter coating.

3. Results and discussion

3.1 Formation of precursor hollow fiber supports comprising silica nanoparticles

To facilitate coating on the precursor, a precursor with only small pores on the top of the sheath layer is required. As is shown in Fig. 3, the nanoparticle containing composite polymer precursor

is composed of a porous nanoparticle containing polymer support core layer and an outer thin sheath layer. The polymer coating solution must not easily penetrate the precursor substrate, otherwise the mass transfer resistance increases after CMS formation. To resist the support densification, nanoparticles were dispersed in the precursor hollow fiber's porous support layer, which forms a porous support layer after the pyrolysis [8]. Fig. 4 shows the as-spun nanoparticle containing precursor hollow fiber membrane, the fiber displayed desirable properties: uniform wall thickness, core layer with open pore structure, and sheath layer with a nanoscopically porous top layer. The thickness of the sheath is around 1.1 µm, which is beneficial to form CMS membrane via pyrolysis to avoid a thick carbon layer with excessive mass transfer resistance. Fig. 4D shows the magnified SEM image of the cross section, a 100 nm thin nanoscopically porous layer at the top of the sheath layer. This layer can effectively suppress the polymer solution penetrating inside the fiber during dip-coating.

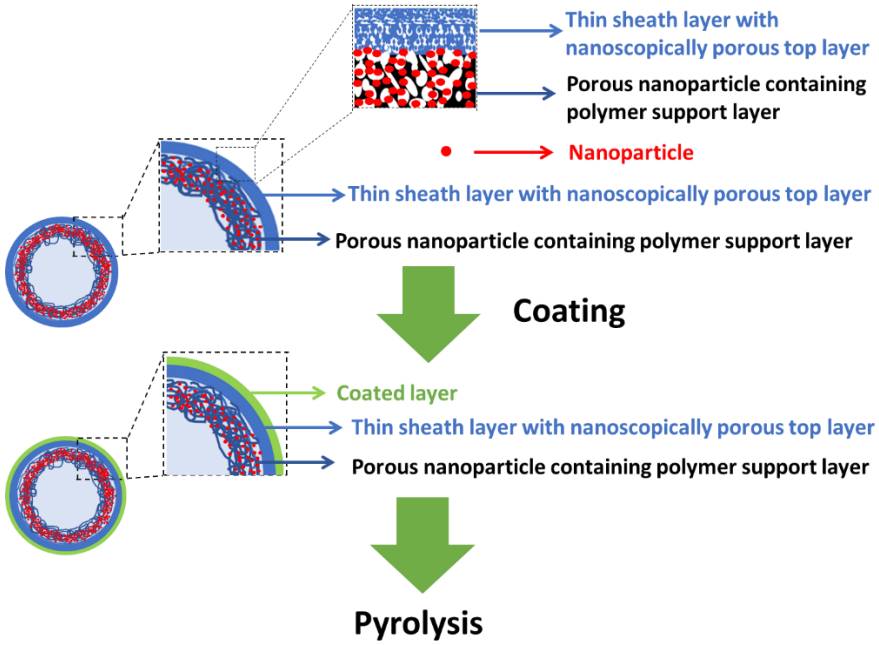

Fig. 3. A schematic illustrating the fabrication of dual-layer composite CMS hollow fiber membranes using dip-coated precursor hollow fibers comprising nanoparticles.

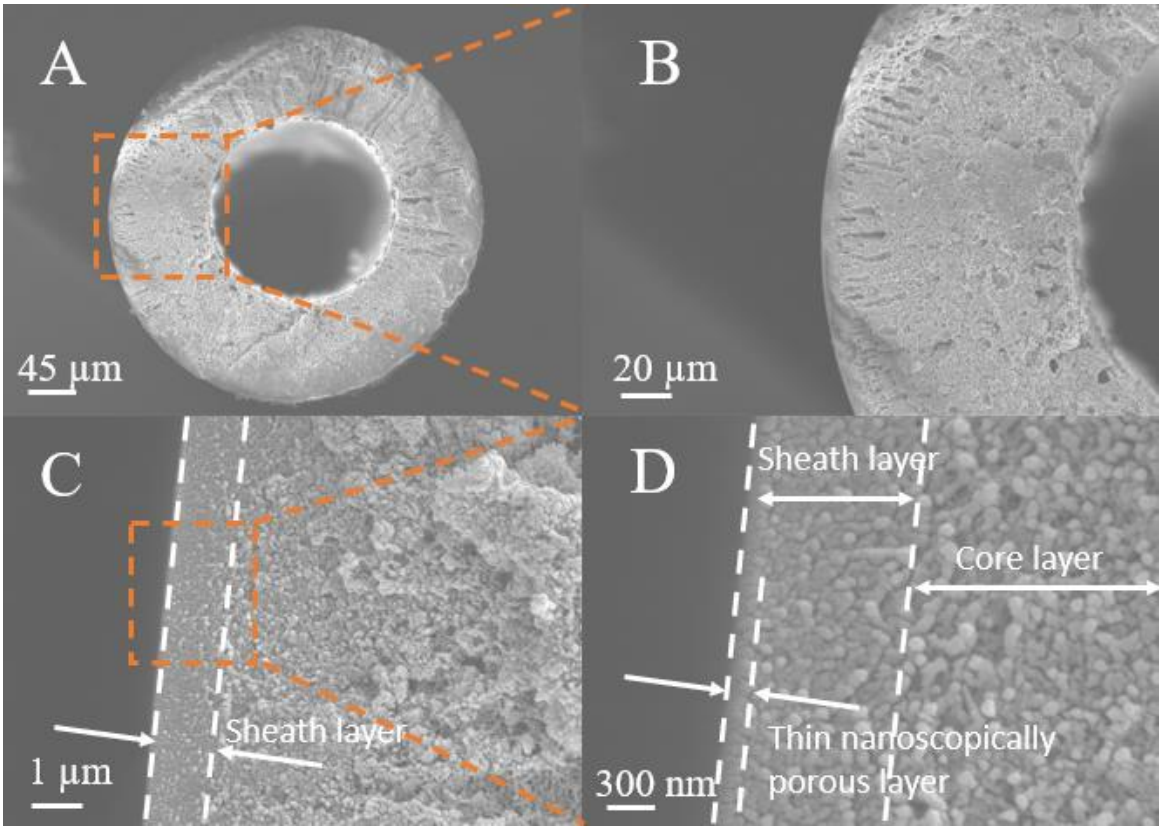

Fig. 4. Cross-sectional scanning electron microscopy of hollow fiber support comprising silica nanoparticles : (A) overall cross-section of a hollow fiber; (B) morphology of the fiber wall; (C and D) the side view of precursor fiber sheath layer.

3.2 Coating 6FDA:BPDA-DAM at high RH

The as spun nanoparticle containing precursor fiber was coated with 4% 6FDA:BPDA-DAM at high RH of 60%. As is shown in Fig. 5A, the coated layer is partially porous. This structure was formed due to the phase separation caused by high RH. CMS membranes were prepared via pyrolyzing the coated precursor at 675 °C and 800 °C, which we name as CMS-4-HRH-675 and CMS-4-HRH-800, respectively. Table 3 shows the permeation results for these CMS membranes. Compared with CMS membranes derived from monolithic 6FDA/BPDA-DAM precursor hollow fibers pyrolyzed at 675 °C (CO_2/CH_4 selectivity of 70), CMS-4-HRH-675 showed lower selectivity (26) possibly due to defects in the separation layer. The defects can be attributed to the partially porous dip coating layer. CO_2/CH_4 selectivity increased from 26.0 to 33.0 while CO_2 permeance dropped from 547.9 GPU to 336.5 GPU when the pyrolysis temperature increased from 675 °C to 800 °C. The results indicate that higher pyrolysis temperature reduces defects in the CMS membrane separation layer by tightenning the carbon membrane matrix during the pyrolysis. Some defects still exist for the CMS membranes generated from coating at high RH. Fig. 5D shows the morphology of the CMS-4-HRH-675 CMS membrane, with some isolated pores (highlighted by yellow circles) apparent in the separation layer, which are eliminated when the pyrolysis temperature was increased to 800 °C. Phase separation induced pore structure appear to cause imperfect separation layer. Such features are not visible for CMS-

4-HRH-800; however, the carbon structure has not tightened enough to give the desired high selectivity. White features in Fig. 5B, Fig. 5C, Fig. 5D and Fig. 5E are silica nanoparticles, which support the carbon matrix in the core layer. Many factors can affect the complex skin layer formation, and understanding the details of such factors is beyond the scope of the current study. We prefer not to speculate on this issue at this point.

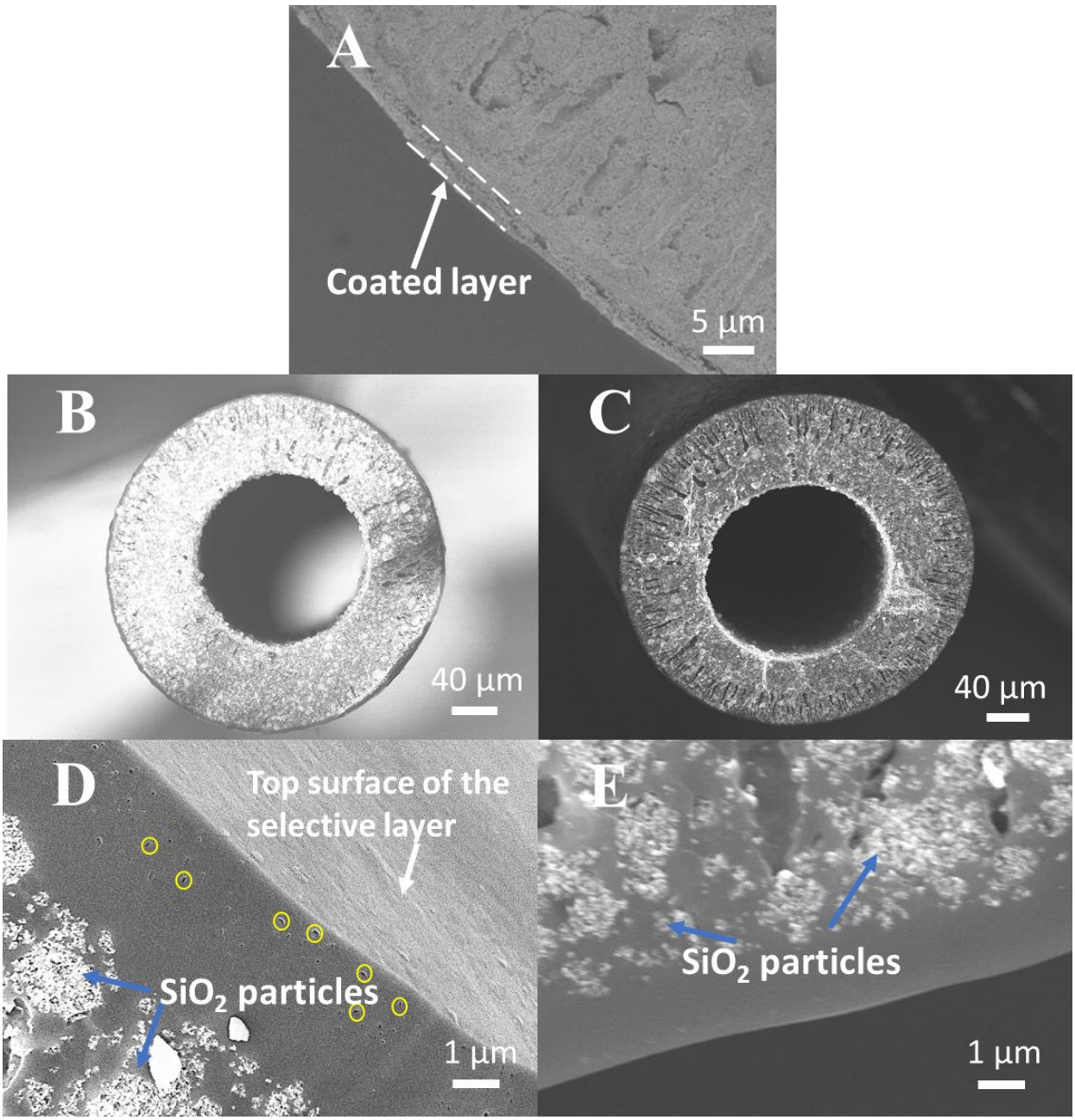

Fig. 5. SEM images of 4% 6FDA:BPDA-DAM coated hollow fiber membranes (at RH 60%): (A) coated precursor fiber membrane; (B and D) CMS membrane prepared from 675 °C pyrolysis; (C and E) CMS membrane prepared from 800 °C pyrolysis.

Table 3. Permeation results of CMS membranes from 4% 6FDA:BPDA-DAM coating at RH 60%.

Sample name	Concentration of the coating polymer solution (wt.%)	Pyrolysis temperature (° C)	CO_2 Permeance (GPU)	Selectivity $\alpha_{CO2/CH4}$
CMS-4-HRH-675	4	675	547.9±86.5	26.0±10.1
CMS-4-HRH-800	4	800	336.5±21.5	33.0±3.0

3.3 Coating 6FDA:BPDA-DAM at low RH

To suppress phase separation during the dip-coating, we investigated dip-coating at low RH. We used three different concentrations of 6FDA:BPDA-DAM polymer solution for the dip-coating at low RH (10%). The SEM images of these coated precursor fiber membranes are shown in Fig. 6. The estimated thickness of the coated layer increased from 120 nm to 200 nm when the 6FDA:BPDA-DAM increased from 2% to 4%. No obvious phase separation was noticed from the coated precursor fiber with different 6FDA:BPDA-DAM concentration.

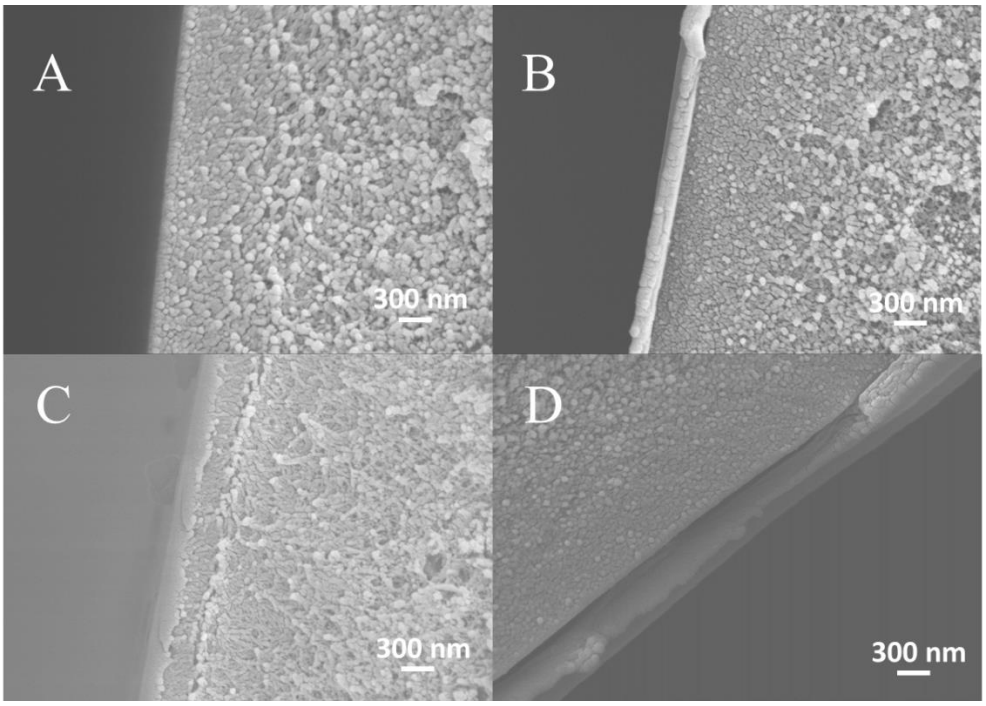

Fig. 6. SEM images of coated hollow fiber membranes with different 6FDA:BPDA-DAM concentration (at RH 10%): (A) 0%; (B) 2%; (C) 3%; (D) 4%.

To investigate effects of polymer concentration on the CMS membrane, 2%, 3% and 4% 6FDA:BPDA-DAM coated precursor at low RH hollow fiber membranes were pyrolyzed at 675 °C. As shown in Table 2, CO_2/CH_4 selectivity increased from 18.1 to 55.7 when polymer solution concentration increased from 2% to 4%, showing a thicker coated layer leads to high

selectivity with defect-free CMS layer. SEM images (Fig. 7) show that higher coating solution concentration gives CMS membranes with thicker separation layers. While the thicker separation layer increased CO_2/CH_4 selectivity, it decreased CO_2 permeance from 606.5 GPU to 199.1 GPU.

Pyrolysis temperature also plays an important role in permeance and selectivity [14]. Different pyrolysis temperatures were employed to investigate the 6FDA:BPDA-DAM coated precursors. As can be seen in Table 2, lower pyrolysis temperature gives lower CO_2/CH_4 selectivity. The permeance of CO_2 is in the order of CMS-4-LRH-550> CMS-4-LRH-675> CMS-4-LRH-800. The highest CO_2/CH_4 selectivity of 80.9 is obtained from CMS-4-LRH-800, with a CO_2 permeance of 189.1 GPU. CMS membranes derived from monolithic 6FDA:BPDA-DAM precursors at 550 °C gives 30-35 for CO_2/CH_4 selectivity with 350 GPU for CO_2 permeance [14]. The CO_2/CH_4 selectivity of CMS-4-LRH-550 is similar to the monolithic derived CMS, while the CO_2 permeance (455.2 GPU) is higher. The support layer of the CMS-4-LRH-550 remains highly open during pyrolysis without densification, as is shown in Fig. 8 A-B. With pyrolysis temperature increasing from 550 °C to 800 °C, the CO_2/CH_4 selectivities increased remarkably to 80.9. This is because the CMS skin structure becomes more tightly packed at high final pyrolysis temperature, resulting in the ultramicropore size distribution shifting to the lower size end[19, 20]. Nevertheless, the supporting layer is still highly open, as is shown in Fig. 8 C-F. This result indicates the nanoparticle supported core layer avoids support densification, which reduced mass transfer resistance compared with traditional monolithic CMS membranes. Comparison to the earlier reported 6FDA:BPDA-DAM composite on a P84 support without nanoparticles, but with a sol-gel treatment to prevent collapse is also useful. Specifically, such a precursor coated at 10% RH with 2% 6FDA:BPDA-DAM and pyrolyzed at 675 °C gave 75.5±2.5 GPU CO_2 and CO_2/CH_4 selectivity of 72.2±0.1 [14]. The previous lower productivity CMS without nanoparticles was not studied at 800°C, like CMS-4-LRH-800, however, it would clearly be less productive but may have higher selectivity, suggesting that optimization and analysis of both types CMS will be valuable.

Table 4. Permeation results of CMS membranes from 6FDA:BPDA-DAM coating at RH 10%.

Membrane name	Concentration of the coating polymer solution (wt.%)	Pyrolysis temperature (°C)	CO_2 Permeance (GPU)	Selectivity $\alpha_{CO2/CH4}$
CMS-2-LRH-675	2	675	606.5±4.5	18.1±0.2
CMS-3-LRH-675	3	675	266.7±59.7	31.2±4.4
CMS-4-LRH-550	4	550	455.2±2.3	33.6±1.8
CMS-4-LRH-675	4	675	199.1±29.1	55.7±11.6
CMS-4-LRH-800	4	800	189.1±27.2	80.9±5.5

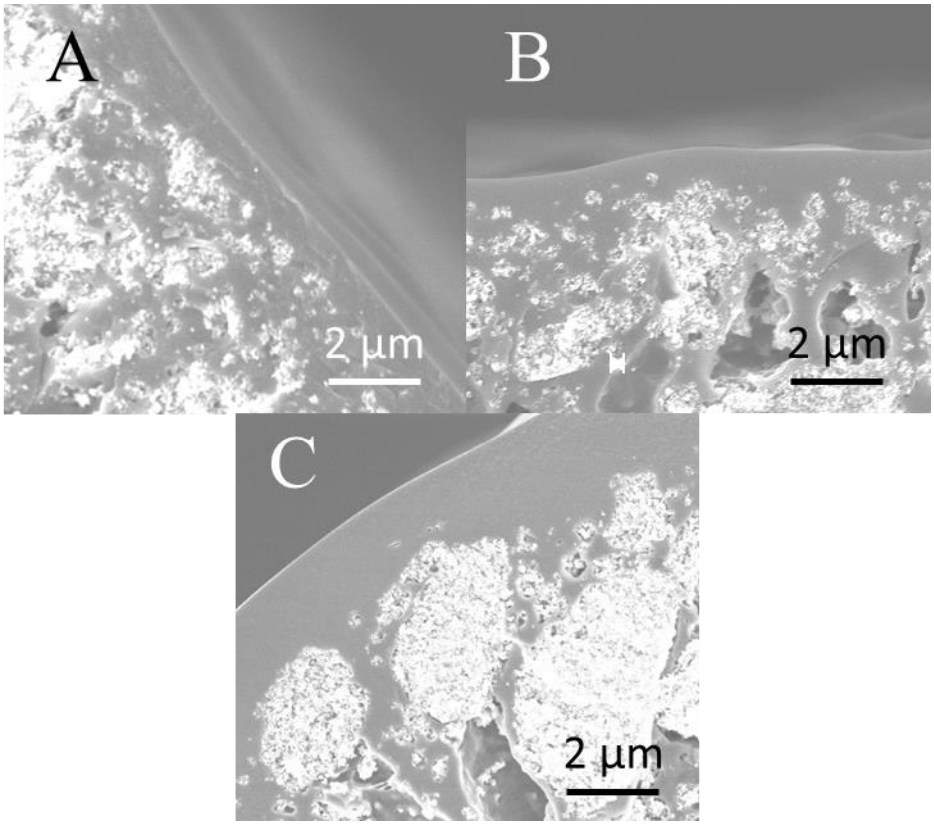

Fig. 7. SEM images of CMS membranes at 675 °C with different 6FDA:BPDA-DAM concentration (at RH 10%): (A) 2%; (B) 3%; (C) 4%.

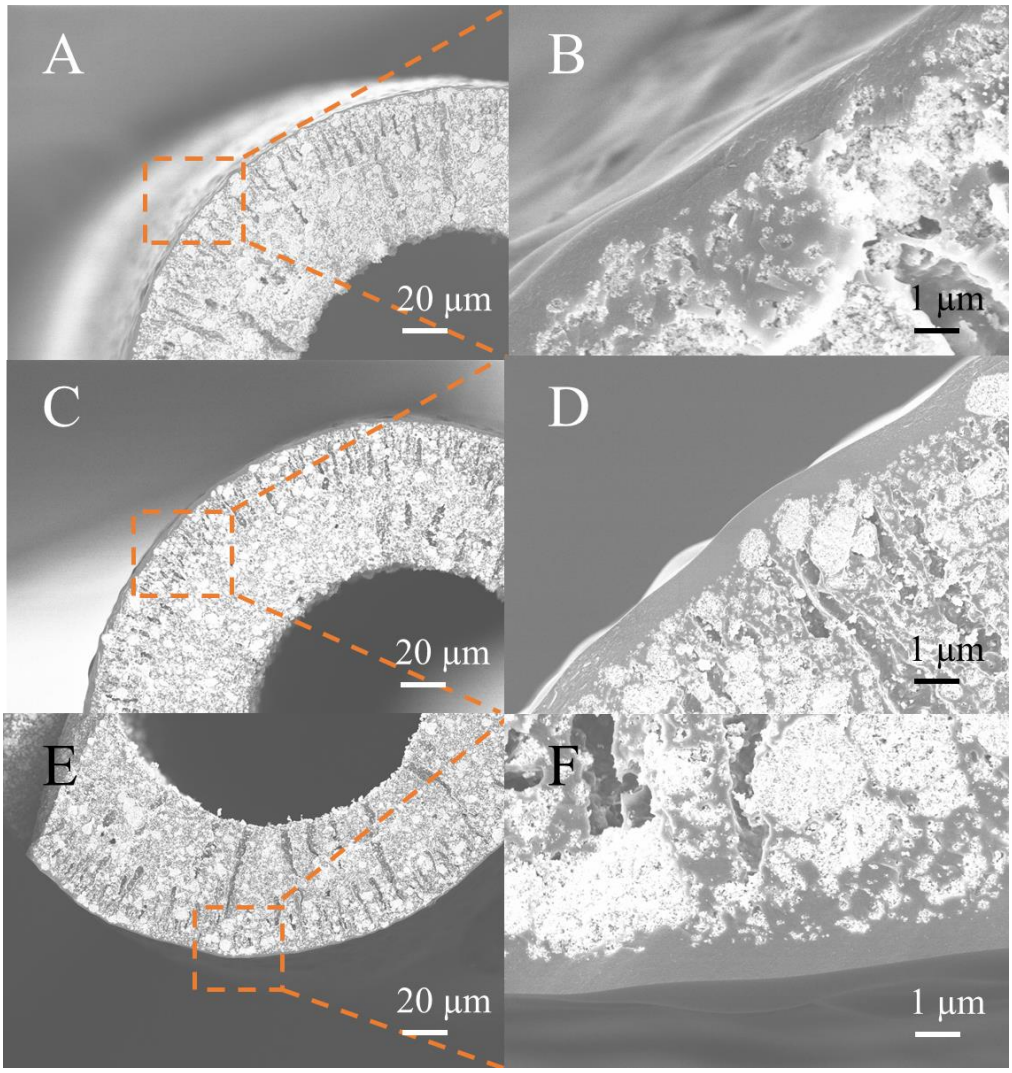

Fig. 8. SEM images of CMS membranes with 4% 6FDA:BPDA-DAM coating at different pyrolysis temperature: 550 °C (A and B); 675 °C (C and D); 800 °C (E and F).

3.4 Coating 6FDA-DAM:DABA (3:2) at low RH

To further demonstrate the versatility of the novel dip-coating approach, a more hydrophilic polymer, 6FDA-DAM:DABA (3:2) was used as the coating polymer. As shown in the Fig. S1, the coated layer has a porous internal structure at high RH using 4% polymer solution, which is similar to the structure we obtained by using 6FDA:BPDA-DAM coating on precursor fiber membranes with and without nanoparticles. However, it is surprising that as-coated precursor membrane derived CMS membrane at 675 °C has a low CO_2/CH_4 selectivity (13.6, shown in Table S1) compared with the 6FDA:BPDA-DAM coated precursor fiber membrane (CO_2/CH_4 selectivity of 26.0). Similar trends have been observed when coating at low RH in Table 3. The 4% 6FDA-DAM:DABA (3:2) coating gave CO_2/CH_4 selectivity of 16.1, which is significantly lower than the CMS CO_2/CH_4 selectivity = 55.7 for 6FDA:BPDA-DAM when coating with the same fabrication.

Table 5. Permeation results of CMS membranes for 6FDA-DAM:DABA (3:2) coating at RH 10%.

Sample name	Concentration of the coating polymer solution (wt.%)	Pyrolysis temperature (°C)	CO_2 Permeance (GPU)	Selectivity $\alpha_{CO2/CH4}$
CMS-DABA-4-LRH-675	4	675	321.6±10	16.1±1.0
CMS-DABA-4-LRH-675-SOAK	4	675	311.2±1.3	21.7 ± 3.6
CMS-DABA-5-LRH-675	5	675	227.6± 20.4	31.8± 2.7
CMS-DABA-5-LRH-675-SOAK	5	675	184.8±1.8	58.9±4.6

conditions. As is shown in Fig. 9A and B, the coating layer is dense with some minor phase separation at low RH. We assume these differences are due to the -COOH groups on the DABA moieties, with higher moisture affinity compared to the 6FDA:BPDA-DAM polymer functional groups. Therefore, the chance of defect formation during the pyrolysis is higher than the 6FDA:BPDA-DAM polymer coating derived CMS membranes. Nevertheless, the higher (5%) coating concentration appears to tighten the nanoscopically porous top layer better than the low coating concentration (4%) at 10% RH. The higher CO_2/CH_4 selectivity for higher coating concentration with the same pyrolysis condition (either with soaking or without soaking at 370 °C) appears adequate, and the dense layer of the resultant CMS membrane is thicker in this case as seen in Fig. 9C, D, E, and F

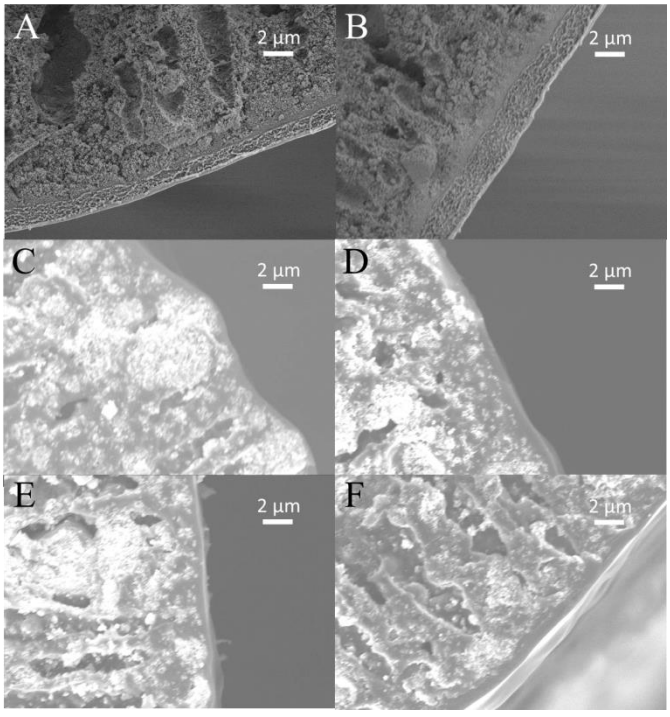

Fig. 9. SEM images of fiber membranes (at RH 10%) coated with 4% 6FDA-DAM:DABA: A) before pyrolysis; C) pyrolyzed with 675℃-no soaking at 370 ℃; E) pyrolyzed with 675℃-

soaking at 370 ℃. Coated with 5% 6FDA-DAM:DABA: B) before pyrolysis; D) pyrolyzed with 675℃-no soaking at 370 ℃; F) pyrolyzed with 675℃- soaking at 370 ℃.

We also hypothesize another reason for the lower CO_2/CH_4 selectivity at the same coating polymer concentration at 675 °C, since the DABA based polyimide can be crosslinked by thermal heating. The suggested mechanism is illustrated in Fig. 10 [15], the decarboxylation-induced crosslinking involves two -COOH groups in DABA moieties reacting to form an anhydride and one water molecule was released [21]. Two phenyl radicals created by decarboxylation of the anhydride can potentially be form the bulky crosslinked structure. The resultant structure can strongly inhibit chain packing, theoretically, having higher permeance compared with the uncross linked precursor derived CMS membrane [1]. However, coated precursor (both 4% and 5%) soaked at 370 ℃ gave CMS with lower permeance and higher CO_2/CH_4 selectivity seen for the 6FDA-DAM:DABA (3:2) at low RH without thermal soaking. It may be that the P84® support layer is a factor in this unusual behavior. The soaking temperature was higher than the Tg of P84® pristine membrane, which is around 320 ℃ [22, 23] and thermal soaking may densify the substructure of the P84® support fiber membrane [23]. Therefore, the defects from the coating layer and sheath layer of the P84® support fiber membrane can be healed better by densification, causing the resultant CMS membranes to have lower permeance and higher CO_2/CH_4 selectivity compared with the CMS membranes without soaking.

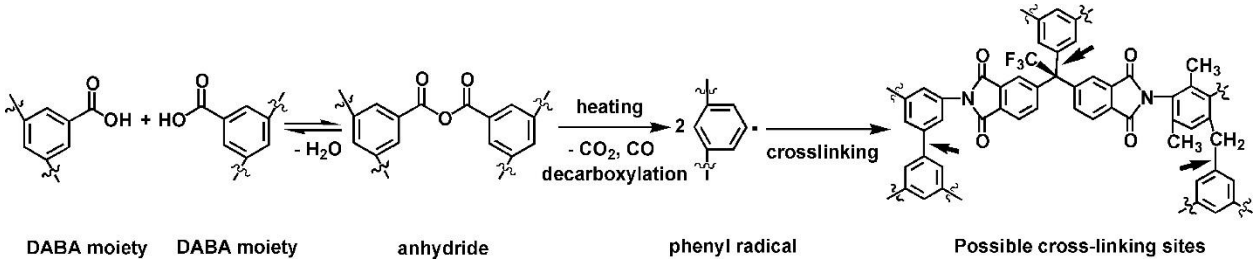

Fig. 10. Decarboxylation-induced cross-linking mechanism and possible cross-linking sites of DABA-based polyimide [15].

As discussed in our previous work [14], CMS membrane preparation by economical coating and pyrolysis of porous polymer hollow fibers in a composite structure can lead to a 25X reduction in expensive precursor polymer material cost.

The two-step process of spinning + dip-coating, has tradeoffs of this technique compared to dual-layer spinning technique, as elaborated below:

1. There is no need to spin defect-free precursor fiber—which greatly decreases the spinning difficulty.

2. The P84 support fiber, when spun independently, provides a versatile platform for dip-coating with various types of high-performance polymers under varied dip-coating conditions (solution concentration, humidity etc.). Essentially, the composite polymer fiber can be tailored as per the application. Fibers spun by the dual-layer technique cannot be tuned in such precise ways prior to pyrolysis.

4. Conclusion

To obtain both high selectivity and permeance of CMS composite fiber, coating a dense skin layer of polymer on the porous support layer fiber was achieved at low RH. The dense skin layer after coating can provide the resultant CMS fiber with high selectivity, while the porous support layer allows high permeance. In the support layer, the low bulk density silicon dioxide occupies a large portion of the volume and maintains the porous structure during pyrolysis, without comprising a large mass fraction of the fiber. SiO_2 nanoparticles are good fillers to make support layer fibers to restrict substructure collapse during pyrolysis. The CMS membrane performance is also highly related to the coating polymer and thermal soaking needs to be applied when 6FDA-DAM:DABA (3:2) was employed to coat the precursor fiber membrane.

Acknowledgment

The authors thank the Office of Basic Energy Science of the U.S. Department of Energy (DE-FG02-04ER15510) for financial support of this work.

Reference:

[1] S. Fu, E.S. Sanders, S.S. Kulkarni, W.J. Koros, Carbon molecular sieve membrane structure–property relationships for four novel 6FDA based polyimide precursors, Journal of Membrane Science 487 (2015) 60-73. https://doi.org/10.1016/j.memsci.2015.03.079.

[2] Y.-J. Fu, C.-C. Hu, D.-W. Lin, H.-A. Tsai, S.-H. Huang, W.-S. Hung, K.-R. Lee, J.-Y. Lai, Adjustable microstructure carbon molecular sieve membranes derived from thermally stable polyetherimide/polyimide blends for gas separation, Carbon 113 (2017) 10-17. https://doi.org/10.1016/j.carbon.2016.11.026.

[3] Z. Wang, H. Ren, S. Zhang, F. Zhang, J. Jin, Carbon Molecular Sieve Membranes Derived from Tröger's Base-Based Microporous Polyimide for Gas Separation, ChemSusChem 11(5) (2018) 916-923. https://doi.org/10.1002/cssc.201702243.

[4] O. Salinas, X. Ma, Y. Wang, Y. Han, I. Pinnau, Carbon molecular sieve membrane from a microporous spirobisindane-based polyimide precursor with enhanced ethylene/ethane mixed-gas selectivity, RSC Advances 7(6) (2017) 3265-3272. https://doi.org/10.1039/c6ra24699k.

[5] Y.-H. Chu, D. Yancey, L. Xu, M. Martinez, M. Brayden, W. Koros, Iron-containing carbon molecular sieve membranes for advanced olefin/paraffin separations, Journal of Membrane Science 548 (2018) 609-620. https://doi.org/10.1016/j.memsci.2017.11.052.

[6] H. Zhao, Y. Cao, X. Ding, M. Zhou, Q. Yuan, Effects of cross-linkers with different molecular weights in cross-linked Matrimid 5218 and test temperature on gas transport properties, Journal of Membrane Science 323(1) (2008) 176-184. https://doi.org/10.1016/j.memsci.2008.06.026.

[7] L. Xu, M. Rungta, W.J. Koros, Matrimid® derived carbon molecular sieve hollow fiber membranes for ethylene/ethane separation, Journal of Membrane Science 380(1-2) (2011) 138-147. https://doi.org/10.1016/j.memsci.2011.06.037.

[8] C. Zhang, K. Zhang, Y. Cao, W.J. Koros, Composite Carbon Molecular Sieve Hollow Fiber Membranes: Resisting Support Densification via Silica Particle Stabilization, Industrial & Engineering Chemistry Research 57(47) (2018) 16051-16058. https://doi.org/10.1021/acs.iecr.8b02386.

[9] N. Bhuwania, Y. Labreche, C.S.K. Achoundong, J. Baltazar, S.K. Burgess, S. Karwa, L. Xu, C.L. Henderson, P.J. Williams, W.J. Koros, Engineering substructure morphology of asymmetric carbon molecular sieve hollow fiber membranes, Carbon 76 (2014) 417-434. https://doi.org/10.1016/j.carbon.2014.05.008.
[10] X. Ma, Y.S. Lin, X. Wei, J. Kniep, Ultrathin carbon molecular sieve membrane for propylene/propane separation, AIChE Journal 62(2) (2016) 491-499. https://doi.org/10.1002/aic.15005.
[11] H.-H. Tseng, C.-T. Wang, G.-L. Zhuang, P. Uchytil, J. Reznickova, K. Setnickova, Enhanced H 2 /CH 4 and H 2 /CO 2 separation by carbon molecular sieve membrane coated on titania modified alumina support: Effects of TiO 2 intermediate layer preparation variables on interfacial adhesion, Journal of Membrane Science 510 (2016) 391-404. https://doi.org/10.1016/j.memsci.2016.02.036.
[12] O. Sanyal, S.T. Hicks, N. Bhuwania, S. Hays, M.G. Kamath, S. Karwa, R. Swaidan, W.J. Koros, Cause and effects of hyperskin features on carbon molecular sieve (CMS) membranes, Journal of Membrane Science 551 (2018) 113-122. https://doi.org/10.1016/j.memsci.2018.01.021.
[13] W. Qiu, C.-C. Chen, L. Xu, L. Cui, D.R. Paul, W.J. Koros, Sub-TgCross-Linking of a Polyimide Membrane for Enhanced CO2Plasticization Resistance for Natural Gas Separation, Macromolecules 44(15) (2011) 6046-6056. https://doi.org/10.1021/ma201033j.
[14] Y. Cao, K. Zhang, O. Sanyal, W.J. Koros, Carbon Molecular Sieve Membrane Preparation by Economical Coating and Pyrolysis of Porous Polymer Hollow Fibers, Angew Chem Int Ed Engl 58(35) (2019) 12149-12153. https://doi.org/10.1002/anie.201906653.
[15] W. Qiu, C.-C. Chen, L. Xu, L. Cui, D.R. Paul, W.J. Koros, Sub-Tg Cross-Linking of a Polyimide Membrane for Enhanced CO2 Plasticization Resistance for Natural Gas Separation, Macromolecules 44(15) (2011) 6046-6056. https://doi.org/10.1021/ma201033j.
[16] S. Fu, E.S. Sanders, S. Kulkarni, Y.-H. Chu, G.B. Wenz, W.J. Koros, The significance of entropic selectivity in carbon molecular sieve membranes derived from 6FDA/DETDA:DABA(3:2) polyimide, Journal of Membrane Science 539 (2017) 329-343. https://doi.org/10.1016/j.memsci.2017.06.007.
[17] S. Fu, G.B. Wenz, E.S. Sanders, S.S. Kulkarni, W. Qiu, C. Ma, W.J. Koros, Effects of pyrolysis conditions on gas separation properties of 6FDA/DETDA:DABA(3:2) derived carbon molecular sieve membranes, Journal of Membrane Science 520 (2016) 699-711. https://doi.org/10.1016/j.memsci.2016.08.013.
[18] C.W. Jones, W.J. Koros, Carbon molecular sieve gas separation membranes-I. Preparation and characterization based on polyimide precursors, Carbon 32(8) (1994) 1419-1425. https://doi.org/https://doi.org/10.1016/0008-6223(94)90135-X.
[19] X. Ning, W.J. Koros, Carbon molecular sieve membranes derived from Matrimid® polyimide for nitrogen/methane separation, Carbon 66 (2014) 511-522. https://doi.org/10.1016/j.carbon.2013.09.028.
[20] C. Zhang, W.J. Koros, Ultraselective Carbon Molecular Sieve Membranes with Tailored Synergistic Sorption Selective Properties, Adv Mater 29(33) (2017). https://doi.org/10.1002/adma.201701631.
[21] M.G. Kamath, S. Fu, A.K. Itta, W. Qiu, G. Liu, R. Swaidan, W.J. Koros, 6FDA-DETDA: DABE polyimide-derived carbon molecular sieve hollow fiber membranes: Circumventing unusual aging phenomena, Journal of Membrane Science 546 (2018) 197-205. https://doi.org/10.1016/j.memsci.2017.10.020.

[22] A. Chong Lua, Y. Shen, Influence of inorganic fillers on the structural and transport properties of mixed matrix membranes, Journal of Applied Polymer Science 128(6) (2013) 4058-4066. https://doi.org/10.1002/app.38614.
[23] L. Sheng, J. Ren, K. Hua, H. Li, Y. Feng, M. Deng, The enhancement of mechanical properties of P84 hollow fiber membranes by thermally annealing below and above Tg, Journal of Membrane Science 595 (2020) 117580. https://doi.org/10.1016/j.memsci.2019.117580.

Graphic abstract